AIAA Paper No. 97-3498

A Theory for the Roll-Ratchet Phenomenon in High Performance Aircraft

Ronald A. Hess[1]
Dept. of Mechanical and Aeronautical Engineering
University of California
Davis, CA 95616

Abstract

Roll-ratchet refers to a high frequency oscillation which can occur in pilot-in-the-loop control of roll attitude in high performance aircraft. The frequencies of oscillation are typically well beyond those associated with the more familiar pilot-induced oscillation. A structural model of the human pilot which has been employed to provide a unified theory for aircraft handling qualities and pilot-induced oscillations is employed here to provide a theory for the existence of roll-ratchet. It is hypothesized and demonstrated using the structural model that the pilot's inappropriate use of vestibular acceleration feedback can cause this phenomenon, a possibility which has been discussed previously by other researchers. The possible influence of biodynamic feedback on roll ratchet is also discussed.

Introduction

Figure 1, taken from Ref. 1 shows two time histories involving the Air Force/CALSPAN NT-33A variable-stability aircraft and the prototype YF-16 vehicle. As the figure indicates, high frequency roll oscillations (*12.17-12.5 rad/s*) occurred under piloted control. Oscillations such as these have been termed *roll-ratchet* by pilots and flight control engineers. The term finds its origin in pilot descriptions of the event, i.e. the pilots often describe what they perceive to be a ratcheting-like motion. The ratcheting sensation may be attributable to a threshold nonlinearity in the human inner ear where acceleration is sensed. While not a dangerous condition, per se, roll ratchet often precludes acceptable performance in air-to-air tracking tasks, and almost invariably leads to a significant degradation in handling qualities ratings.

There has been a considerable amount of research devoted to seeking the mechanism behind the roll ratchet phenomenon, e.g. Refs. 1-6. Perhaps one of the first explanations of the phenomenon was offered in Ref. 2, and discussed in some detail in Ref. 1. The authors of Ref. 2 were the first to suggest the importance of acceleration cues in catalyzing roll ratchet:

> *"Suppose the pilot reverts to an abrupt input technique to demand the desired response more rapidly, creates high angular accelerations and then switches his closure to angular acceleration error, instead of bank angle error. Then with sufficient pilot gain, a ratcheting type oscillation of ≃ 16 rad/s results."*

While recognizing the importance of acceleration cues, other researchers have maintained that the interaction of the pilot's neuromuscular system and the cockpit control inceptor are the important factors in understanding roll-ratchet, e.g. Refs. 3 and 5. Consider Fig. 2 from Ref. 3. This figure shows the Bode plots of a series of measured pilot-vehicle transfer functions from a fixed-base simulation of a roll tracking task when a force-sensing cockpit inceptor was being used, i.e. the force which the pilot applied was sensed and used as a command to the vehicle and/or flight control system. The amplitude peaking evident just beyond 10 rad/s should be noted. To induce an oscillatory response, the phase lag at the frequency where this amplitude peak crosses the *0 dB* line has to be reduced to *-180 deg*. The authors hypothesize that the pilot's use of motion cues provides this phase lag reduction. In Fig. 2, the $0.1\omega \times 57.3$ is the phase *lead* which the authors state can be provided by "inner-loop" roll-rate feedback. The authors conclude that avoiding the use of force-sensing cockpit inceptors can minimize

[1]Professor, Associate Fellow AIAA

the occurrence of roll ratchet, a conclusion also reached in Ref. 5.

More recent flight test results have demonstrated that merely avoiding force command inceptors is not sufficient to prevent the occurrence of roll ratchet. In Refs. 4 and 6, flight test data from the Air Force/CALSPAN NT-33A variable-stability aircraft demonstrated that roll ratchet can occur with either position or force-sensing inceptors. The data from these references is particularly interesting in that pilot-vehicle transfer functions, like that shown in Fig. 2 were measured in tracking tasks involving sum-of-sinusoids roll-command inputs. The interpretation of this data, however, varies. That is, referring to the work of Refs. 3 and 5, there is some evidence that neuromuscular mode peaking is occurring with roll ratchet, but it is not always present in the transfer functions where ratchet is occurring. This, of course, can be explained by the fact that ratcheting is a sporadic event, and describing functions are time-averaged linearizations of the entire tracking sequence. Thus, those periods when ratchet did not occur were averaged with those where it did, and the result shows evidence of peaking, but no ratchet.

A Model-Based Theory for Roll Ratchet

Introduction

The explanations for roll-ratchet briefly described in the preceding paragraph, while plausible, suffer from the fact that they require some rather special conditions to be met for their validity. For example, the theory forwarded in Refs. 1 and 2 requires the pilot to visually sense the *second* derivative of the system error, not an easy task based upon what is known of human pilot visual sensing capabilities. The work reported in Ref. 3 indicates that conditions can occur in which the amplitude of the neuromuscular mode peak is near or at unity (*0 dB*), at the frequency where the phase lag is near or at *-180 deg*. These conditions are those which would imply a high-frequency, closed-loop oscillation.

The explanation to be proposed herein, draws upon both of the previous hypotheses to some extent. However, it is based upon a simple model of the human pilot which has been used to provide a unified theory for aircraft handling qualities and pilot-induced oscillations.[7] As will be seen, with this model the phenomenon of roll-ratchet can be explained by the pilot's use of an inappropriately large feedback gain on roll acceleration sensed through the vestibular system.

The Revised Structural Model

Figure 3 shows what will be referred to here as the "revised structural model" of the human pilot. The model has its genesis in a previously described structural model, e.g., Ref. 8, and in a later modification of that model.[5] As shown in Fig. 3, the model is describing *compensatory pilot behavior*, i.e., behavior involving closed-loop tracking in which the visual input is system error. The elements within the dashed box represent the dynamics of the human pilot.

The model of Fig. 3 is discussed thoroughly in Ref. 7, and part of that discussion is repeated here for the sake of completeness. Starting from the left, one sees the system error $e(t)$ following one of two possible paths. One path is intended to model the human's visual rate-sensing dynamics, here modeled by a differentiator (s), an injected noise signal, and a gain K_i. The remaining path describes normal error sensing and gain compensation K_e, including the possibility of the human's accomplishing low-frequency trim (or integral) compensation via ϵ/s. In this study, $\epsilon \equiv 0$. The switch labeled S_1 allows switching between error and error-rate tracking. This switching has been hypothesized to play a critical role in the initiation and sustenance of pilot-induced oscillations.[7] Switches S_1 and S_2 are assumed to operate in unison, i.e., when S_1 is in the "up" position, so is S_2. For this study, however, it is assumed switches S_1 and S_2 remain in the "down" position and normal error sensing and compensation is used. A central processing time delay τ_0 is also included. An inner, proprioceptive feedback loop is encountered next. In the forward portion of this loop, the elements Y_{NM} and Y_{FS} are intended to represent, respectively, the open-loop dynamics of the neuromuscular system driving the cockpit inceptor, and the dynamics of the inceptor force-feel system, itself. The feedback portion of this loop contains the element Y_{PF}, which receives as its input the proprioceptively sensed inceptor output $\delta_m(t)$. The element Y_{PF} and its position in the model is central to the philosophy of the structural model, i.e., that the primary equalization capabilities of the human pilot are assumed to occur through operation upon a proprioceptively sensed, as opposed to a visually sensed, variable. The switch S_3 allows either *position-sensing* or *force-sensing* inceptors

to be modeled.

Time derivatives of the vehicle output $m(t)$ are assumed to be individually sensed as indicated in Fig. 3. Switch S_4 allows either rate or acceleration cues or neither to be used in vehicular control. It should be noted that feeding back output *rate* is predicated on that signal creating an *acceleration* which can be sensed by the middle ear. In this study, $K_{\dot{m}} = 0$. A visual feedback of vehicle output completes the model.

Model Parameterization

The reader is referred to Ref. 7 for a discussion of model parameterization, which will only be summarized here. Elements Y_{NM} and Y_{PF} are given by

$$Y_{NM} = \frac{\omega_{NM}^2}{s^2+2\zeta_{NM}\omega_{NM}s+\omega_{NM}^2} \tag{1}$$

$$Y_{PF} = \begin{cases} K(s+a) & or, \\ K & or, \\ K/(s+a) \end{cases} \tag{2}$$

with the particular equalization of Eq. 2 dependent upon the form of the vehicle dynamics around the crossover frequency. The crossover frequency is chosen as 2.0 rad/s.

Nominal values for "fixed" model parameters can be given as

$$\begin{aligned} \tau_0 &= 0.2\ s \\ \omega_{NM} &= 10\ rad/s \\ \zeta_{NM} &= 0.7 \end{aligned} \tag{3}$$

The relatively simple relations of Eqs. 1-3, the crossover relation $\omega_c = 2.0\ rad/s$ and the selection of one of the three forms on the right hand side of Eq. 2 allow implementation of the model of Fig. 3. The appropriate form in Eq. 2 is chosen so that the resulting open loop transfer function

$$Y_p Y_c(j\omega) = \frac{\delta_M}{E}(j\omega)\cdot Y_c(j\omega) \approx \frac{\omega_c}{j\omega}e^{-\tau_e s} \quad for\ \omega \approx \omega_c \tag{4}$$

i.e., $Y_p Y_c(j\omega)$ follows the dictates of the crossover model of the human pilot.[9] The gain K appearing in Eq. 2 is chosen so that, with all other loops open, the minimum damping ratio of any quadratic closed-loop poles of $\frac{\delta_M}{E_M}(s)$ is $\zeta_{min} = 0.15$. Finally, K_e is selected so that the desired crossover frequency of *2.0 rad/s* is obtained. As will be demonstrated, the inclusion of a nonzero $K_{\dot{m}}$ (with switch S_4 in the "up" position) can alter the high-frequency characteristics of the open-loop transfer function $\frac{M}{E}(s)$ and produce oscillatory behavior very similar to that seen in roll ratchet. The inclusion of a nonzero $K_{\dot{m}}$ *after* selection of K_e in the modeling procedure described in the preceding is possible since $K_{\dot{m}}$ has only a small effect upon the crossover frequency.

Analysis of Roll Ratchet

Data Base

The data to be used is taken from that presented in Ref. 4 and discussed in Ref. 6. It involves a series of roll-tracking tasks conduced on the Air Force/CALSPAN NT-33A variable stability aircraft. Attention will be focused upon eleven configurations which have been identified in Ref. 6 as either not experiencing or experiencing roll-ratchet in flight test. Figure 4 describes the short-hand notation used to identify the configurations. The eleven configurations analyzed are shown in Table 1.

It is useful to provide some validation of the structural model and parameter selection procedure described in the preceding. To this end, a comparison can be made between a pilot-vehicle transfer function obtained from flight test and one generated by the structural model. Configuration *221P(18)* was selected for comparison. Figure 5 shows the flight test and model results. In terms of the variables in Fig. 3, Fig. 5 is a Bode plot of $\frac{M}{E}(j\omega)$. The shaded circles represent magnitude and phase measurements from flight test at the frequencies of the command input sinusoids comprising $c(t)$ while the solid and dashed

curves represent the model results. The model was obtained using the pilot-vehicle analysis technique outlined in the preceding *with one exception*: the crossover frequency for the model pilot-vehicle system was reduced from *2.0 rad/s* to *1.5 rad/s* to provide an acceptable match to the amplitude data and allow an easier comparison with this data. As the figure indicates, with the one exception of the crossover frequency the comparison is quite good. The crossover frequency discrepancy was not deemed serious, and will be ignored in what follows.

Acceleration Feedback

The simple hypothesis offered here is that the roll-ratchet phenomenon can be induced by the pilot adopting an inappropriately large gain $K_{\dot{m}}$. It is further hypothesized that this large gain is induced by rolling accelerations created by the aircraft and flight control system which the pilot deems excessive for the task at hand. This latter hypothesis is identical to that offered in Refs. 1 and 2. The difference, however, is that the acceleration sensing occurs in a feedback loop, through the vestibular system and is *not* occurring through visual means in the forward-loop. The interplay of the neuromuscular system and the nature of the force-feel system is obvious from the structure of the proprioceptive feedback loop in Fig. 3. Thus, this hypothesis has many of elements in common with that offered in Ref. 3. However, as will be demonstrated, only a single gain variation need be employed to induce a closed-loop oscillation very similar to a roll-ratchet.

Figure 6 shows the structural model pilot-vehicle transfer function for configuration *143P(18)* with two values of $K_{\dot{m}}$, zero and a value yielding a very lightly-damped high-frequency mode. It should be noted that such a gain increase may only be transient, i.e. it may not occur over a long enough period of time to be accurately captured by a single transfer function measurement such as that shown in Fig. 5. Also note in Fig. 6, that there is only a modest change in crossover frequency with the non-zero $K_{\dot{m}}$. Finally, the closure of the outer, visual loop in Fig. 3 has little effect upon the relative stability of the oscillatory mode. This is shown in the root locus diagram of Fig. 7. Here, the open-loop transfer function $\frac{M}{E}(s)$ includes the acceleration loop closed with the non-zero $K_{\dot{m}}$. The small squares indicate closed-loop root locations, i.e., poles of the transfer function $\frac{M}{C}(s)$, for four values of the "visual" gain K_e. These correspond to factors of *1, 2, 5,* and *10* times the nominal value which yielded the *2.0 rad/s* crossover frequency with $K_{\dot{m}} = 0$. Note the very small change in the position of the oscillatory "roll-ratchet" roots. Taking the model at face value, this result means that the pilot cannot stop a roll-ratchet by varying his/her outer-loop, "visual" gain, K_e. The ratchet can only be stopped by a reduction in $K_{\dot{m}}$. It is interesting to compare this result with that implied by Fig. 2 and Ref. 3. There, the existence of a roll-ratchet is predicated upon an appropriate outer-loop gain which forces the magnitude of the open-loop transfer function to be unity (*0 dB*) at the frequency at which the phase angle is *-180 deg*. A similar statement can be made about the model proposed in Ref. 1.

Figure 8 shows a the output $m(t)$ and the force input $\delta_F(t)$ to a unit step input for configuration *143P(18)*. This pair of time histories are interesting in that they are qualitatively similar to recorded roll-ratchet time histories. That is, only a small amplitude oscillation is evident in roll-attitude, while a large amplitude oscillation is evident in control input. Figure 8 shows the pilot control force input during flight-test roll-ratchet encounter with configuration *143P(18)*. The frequency of oscillation is *10.4 rad/s*, while that obtained with the model is *9.8 rad/s*.

The inappropriately large gain $K_{\dot{m}}$ may be attributed to the following: In maneuvering, the particular flight configurations which are prone to roll ratchet, create a rolling acceleration which the pilot finds excessive for the task at hand. This may occur even if the task itself involves relatively modest accelerations in an absolute sense. If a physiological sensor is available to measure this acceleration (which it obviously is), the natural tendency on the part of the pilot may be to feedback this variable and attempt to reduce it through control activity. However, because of the structure of the pilot's feedback system, this action merely leads to a very lightly damped mode and a roll ratchet.

Vehicle Characteristics

If initial acceleration response is involved in the initiation of roll ratchet, it may be possible to distinguish some differences in open-loop acceleration response to applied force inputs, at least for the eleven

configurations of Table 1. To this end, the transfer function $\left[s^2 \cdot \frac{M}{\delta_F}(s)\right]_{s=j\omega}$ was plotted for each set of configurations in Table 1, i.e., those with no ratchet and those with ratchet. Note that this transfer function will contain just vehicle, actuator and force-feel system dynamics when a position-sensing inceptor is being used, and vehicle and actuator dynamics, alone, when a force-sensing actuators is being used. Note that no pilot dynamics are included. Figures 10 and 11 summarize the results. Since it is the *initial* acceleration response which is of interest ($t << 1$), attention should be focused on the characteristics of $\left[s^2 \cdot \frac{M}{\delta_F}(s)\right]_{s=j\omega}$ for values of $j\omega$ which are large but do not exceed the upper limit of the frequency range of interest for manual control, i.e., $\omega \approx 10$ *rad/s*. Figure 10 shows $\left[s^2 \cdot \frac{M}{\delta_F}(s)\right]_{s=j\omega}$ for the configurations which did not exhibit roll ratchet, while Fig. 11 shows the function for those that did. Even for this small data set, some basic differences appear. The no-ratchet cases all had phase lags at *10 rad/s* which were less than *-75 deg* i.e., less negative. In contrast, all but one of the ratchet cases had phase lags greater than *-75 deg* i.e., more negative. The configuration in Fig. 11 which did not have a phase lag at *10 rad/s* exceeding *-75 deg* did, however, have a relatively large magnitude at this frequency. The magnitude and phase for this configuration (*201P(18)+55*) are denoted by arrows in Fig. 11. The one configuration in Fig. 10 which comes close to exceeding *-75 deg* (*342P(18)*) also exhibits the smallest magnitude in the high frequency range. This pair is also denoted by arrows in Fig. 10. It is interesting that of the two piloted evaluations of configuration (*342P(18)*) reported in Ref. 4, one of the pilots reported no roll ratchet and gave the configuration a Cooper-Harper rating of 2. The second pilot, however, did report some oscillation problems that he found objectionable, but said that there were *no* PIO problems. He gave the configuration a Cooper-Harper rating of 5 because of these oscillations. It is not known for certain whether these oscillations were roll ratchet, however, one might expect that they were since the pilot explicitly exonerated the vehicle from PIO tendencies (which are typically categorized by pilots as being of lower frequency than roll-ratchet). Thus, the "close-call" for configuration *342P(18)* in Fig. 10 may be reasonable. These results support an hypothesis that *initial* acceleration responses to force inputs that exhibit large lags or large amplitudes in the frequency domain may induce the pilot to employ an inappropriately large acceleration feedback gain in an attempt to control the resulting response. As an example of such responses in the time domain, Fig. 12 compares the time-domain roll acceleration responses to step applied forces for configurations *301P(18)* (no ratchet) and *143P(18)* (ratchet). Figures 10 and 11 also show a pair of phase-amplitude boundaries which can be used to delineate the roll-ratchet proneness of these configurations. That is, if a the magnitude or phase of $\left[s^2 \cdot \frac{M}{\delta_F}(s)\right]_{s=j\omega}$ violates either of these bounds, the configuration experienced roll-ratchet in flight test. Of course, it is presumed that some minimum magnitude of $\left[s^2 \cdot \frac{M}{\delta_F}(s)\right]_{s=j\omega}$ at *10 rad/s* would be required to induce roll ratchet. The relatively small data set of Table 1 does not permit an estimate of this lower bound.

Biodynamic Feedback

A discussion of the roll-ratchet would not be complete without considering the possible role which biodynamic feedback may play in the phenomenon. The terms biodynamic or biomechanical feedback are used here to imply the effects which vehicle roll acceleration might have on the pilot's arm and cockpit inceptor, and how these effects may serve to catalyze roll ratchet.

A very simple model of biodynamic feedback can be obtained by considering the pilot's hand/arm and the inceptor grip as consisting of an effective point mass m_e a distance r above the instantaneous roll axis of the aircraft.[5] Consider the situation in which both the control stick pivot point and the location of the effective point mass are above the instantaneous roll-axis of the aircraft. When the aircraft is undergoing a rolling maneuver with roll acceleration $\ddot{\phi}$, the force which the pilot must apply to keep the inceptor from moving relative to the cockpit is simply $-rm_e\ddot{\phi}$. To account for dynamics obviously neglected in this simple model, one can consider the biodynamic element to be $rm_e s^2 e^{-\tau s}$, where the time delay τ accounts, in a rudimentary way, for the phase effects of neglected higher frequency dynamics in the biodynamic model.

Figure 13 shows how the structural model of Fig. 3 can be modified to incorporate this rudimentary model of biodynamic feedback.

Figure 14 shows the root locus diagrams for the closed-loop poles of the $\frac{M}{E_M}(s)$ transfer function from Figs. 3 or 13, with τ = 0.025, 0.05, and 0.1 s with vehicle dynamics and model parameters (Y_{PF}) for Config. *143P(18)*. The closed-loop poles in Fig. 14 correspond to those values of rm_e chosen to produce oscillatory roots. For the case when τ = 0.1 s the frequency of the oscillatory mode is 11.4 rad/s, close to roll-ratchet frequency of 10.4 rad/s obtained in flight test for Config. *143P(18)*. An open-loop transfer function very similar to that indicated by the solid curves in Fig. 6, was obtained for the case with biodynamic feedback and τ = 0.1 s, a result which is not too surprising seeing that the same variable is being fedback in both cases, albeit into different locations in the pilot model.

Figure 14 suggests that biodynamic feedback may, itself, produce oscillatory behavior of the kind and frequency associated with roll ratchet. However, one must bear in mind that the "gain" on the root locus diagrams of Fig. 14 is not a variable quantity as in the case of $K_{\dot{m}}$, but rather a geometrical/biomechanical constant, whose value is a function of the mass distribution of the control inceptor, the mass, position and tension of the muscle groups subject to motion under acceleration, and the position of the aircraft's instantaneous roll axis. While it is certainly possible that these quantities may produce oscillatory root locations, it would appear to the author to be less likely than in the case of acceleration feedback via $K_{\dot{m}}$. Finally, it should be noted that conditions which would increase the likelihood of biodynamically-induced roll ratchet, e.g. lack of sufficient arm support, and/or lack of a mechanical break-out in a control inceptor, are also conditions which would adversely affect the operation of the hypothesized proprioceptive loop in Fig. 3. This, in turn, could induce the pilot to use acceleration feedback in an attempt to ameliorate roll accelerations produced by control stick inputs of less precision than desired.

Discussion

The previous analysis is obviously not exhaustive in terms of configurations analyzed. It was intended to demonstrate that a theory could be proposed to explain the origins of the roll-ratchet phenomenon that was consistent with previous observations and could be part of a larger theory which has attempted to unify aircraft handling qualities and the lower frequency phenomena typically identified as pilot-induced oscillations.[7] It is not proposed that the boundaries shown in Figs. 10 and 11 be considered as a metric for assessing the roll-ratchet proneness of any vehicle. One obvious reason for this is that different vehicles will induce different accelerations to identical control force inputs due merely to different pilot station locations. The fact that the eleven configurations of Table 1 were created on the same test vehicle made the comparisons of Figs. 10 and 11 possible. As stated in the previous section, these figures merely support the idea that the characteristics of initial acceleration response may be a key factor in initiating roll ratchet. Finally, the possibility that biodynamic feedback may act as a catalyst for roll-ratchet is certainly plausible, but is felt to be a less-likely explanation than the theory proposed.

Conclusions

A theory for the roll-ratchet phenomenon can be forwarded which is based upon a revised structural pilot model. The theory states that roll-ratchet is caused by the pilot's inappropriate use of vestibular acceleration feedback. The proposed theory contains elements found in previous explanations of roll ratchet, i.e., the importance of acceleration cues and the influence of the pilot's neuromuscular dynamics. Using the structural model, one can create oscillations whose frequency closely approximates that found in flight test of roll-ratchet prone aircraft. In addition, the nature of the time histories which can be produced by the model are qualitatively similar to those found in flight test, i.e., small amplitude oscillations in roll-attitude time histories, but strong evidence in control input time histories. As opposed to other model-based explanations for roll ratchet, the structural model implies that the pilot cannot halt a roll ratchet encounter by changes in his/her visual gain, but only by reduction in the vestibular acceleration feedback gain. For the series of flight tests analyzed, the nature of the initial (open-loop) acceleration response of the vehicle could be used to categorize the roll-ratchet proneness in the eleven configurations chosen for study. Biodynamic feedback was modeled in rudimentary fashion and found to be a plausible but, in the author's opinion, a less-likely candidate for catalyzing roll ratchet. At present, the data base is not sufficient to delineate

Acknowledgement

This research was supported by NASA Langley Research Center under grant No. NAG1-1744. Dr. Barton Bacon was the contract technical manager.

References

[1]Chalk, C. R., "Excessive Roll Damping Can Cause Roll Ratchet," *Journal of Guidance, Control and Dynamics*, Vol. 6, No. 3, 1983, pp. 218-219.

[2]Smith, R. E., Monagan, S. J., and Bailey, R. E., "An In-flight Investigation of Higher Order Control System Effects on the Lateral-Directional Flying Qualities of Fighter Airplanes," AIAA Paper No. 81-1891, 1981.

[3]Johnston, D. E., and Aponso, B. L., "Design Considerations of Manipulator and Feel System Characteristics in Roll Tracking," NASA CR-4111, Feb., 1988.

[4]Bailey, R. E., and Knots, L. H., "Interaction of Fell System and Flight Control System Dynamics on Lateral Flying Qualities," NASA CR-179445, Dec. 1990.

[5]Hess, R. A., "Analyzing Manipulator and Feel System Effects in Aircraft Flight Control," *IEEE Transactions on Systems, Man, and Cybernetics*, Vol. 20, No. 4, 1990, pp. 923-931.

[6]Mitchell, D. G., Aponso, B. L., and Klyde, D. H., "Effects of Cockpit Lateral Stick Characteristics on Handling Qualities and Pilot Dynamics," NASA CR-4443, June, 1992.

[7]Hess, R. A., "A Unifying Theory for Aircraft Handling Qualities and Adverse Aircraaft-Pilot Coupling," *Journal of Guidance, Control, and Dynamics*, to appear.

[8]Hess, R. A., "A Model for the Human's Use of Motion Cues in Vehicular Control," *Journal of Guidance, Control, and Dynamics*, Vol. 13, No. 3, 1990, pp. 476-482.

[9]McRuer, D. T. and Krendel, E. S., "Mathematical Models of Human Pilot Behavior, AGARDograph-AG-188, 1974.

Table 1 Flight Test Configurations Analyzed from Ref. 4

no roll ratchet	roll ratchet
141F(10)	143P(18)
301P(18)	201P(18)+55
302P(18)	221P(18)
341F(18)	301P(18)+110
342P(18)	302P(18)+55
342F(18)	

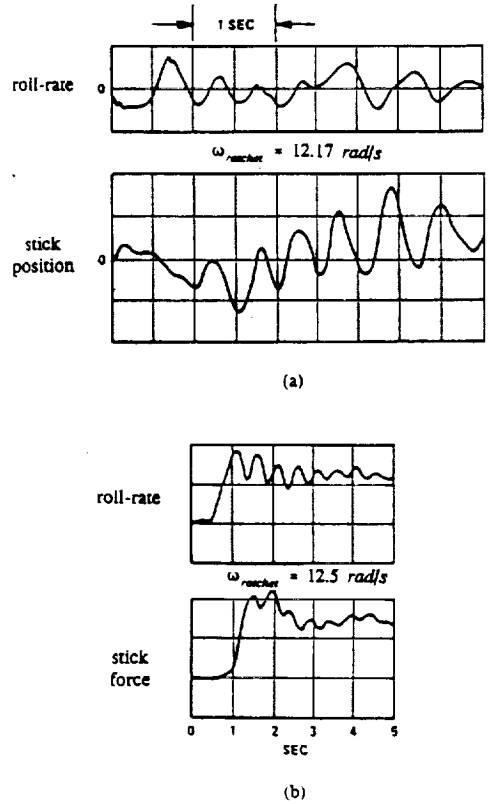

Fig. 1 Roll ratchet time histories; (a) NT-33A, (b) YF-16.

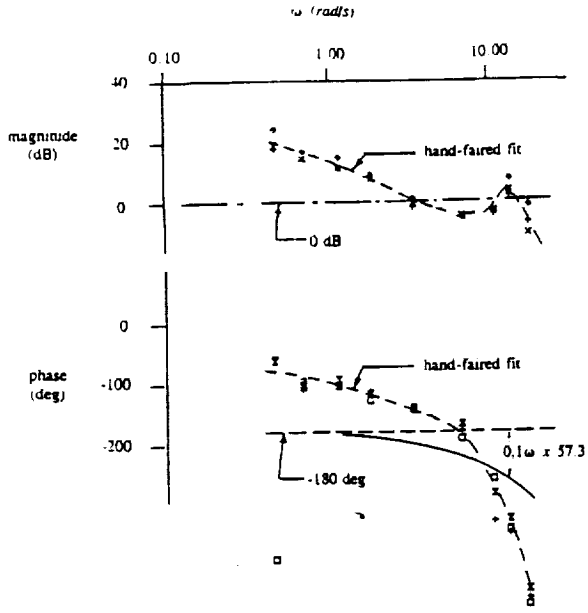

Fig. 2 Measured pilot-vehicle transfer function characteristics from Ref. 3.

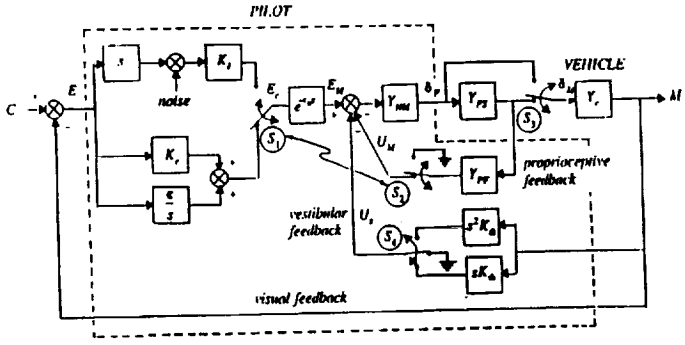

Fig. 3 A revised structural model of the human pilot.

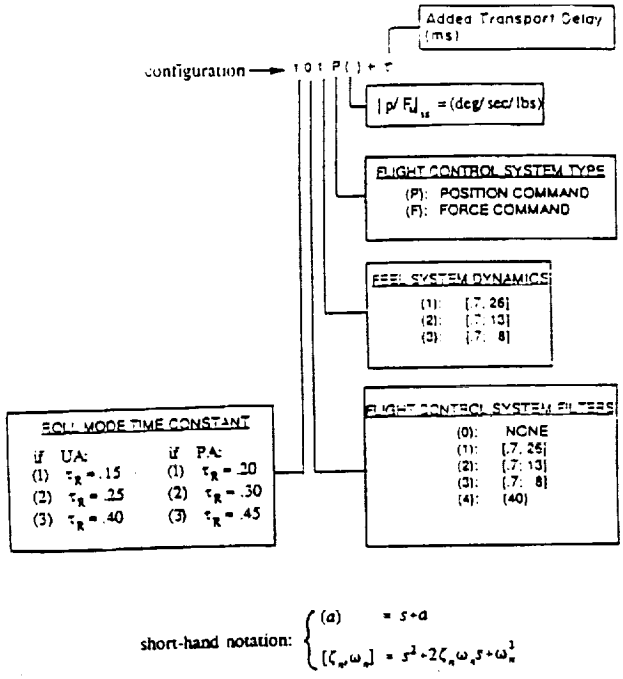

Fig. 4 Configuration identification scheme from Ref. 6.

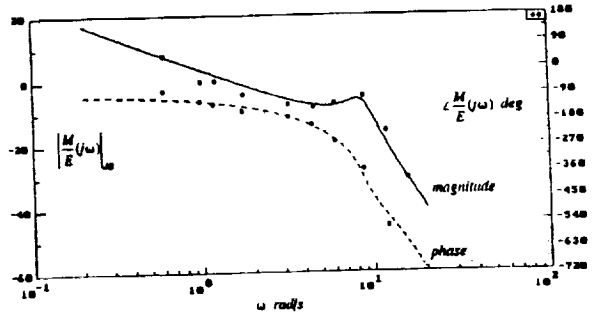

Fig. 5 Comparison of pilot-vehicle transfer functions from flight-test and structural model; Configuration *221P(18)*.

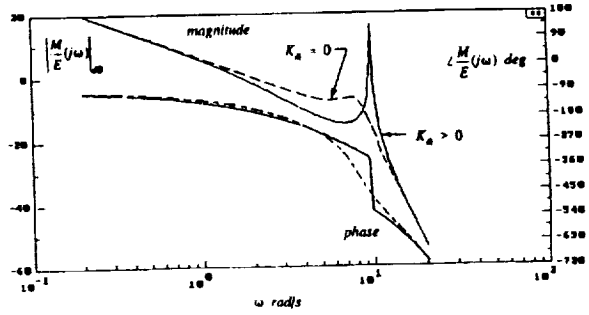

Fig. 6 Structural model pilot-vehicle transfer function with two values of $K_{\dot{m}}$; Configuration *143P(18)*.

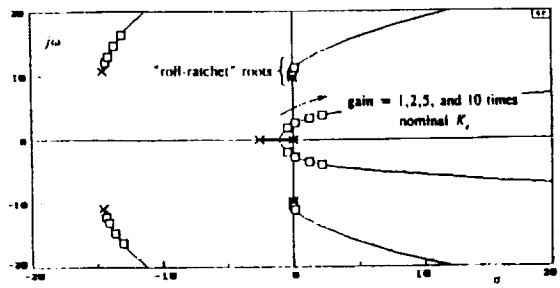

Fig. 7 Root locus diagram for closed-loop poles of $\frac{M}{C}(s)$ with open-loop transfer function $\frac{M}{E}(s)$ defined with non-zero K_{rr} of Fig. 6. Closed-loop roots correspond to varying nominal K_e by factors of 1, 2, 5, and 10.

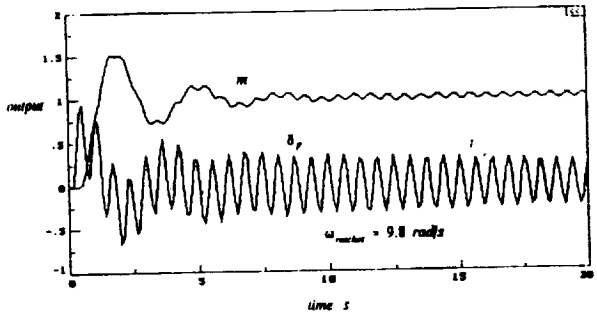

Fig. 8 Closed-loop step response of pilot-vehicle system of Fig. 3, with pilot-vehicle transfer function of Fig. 6.

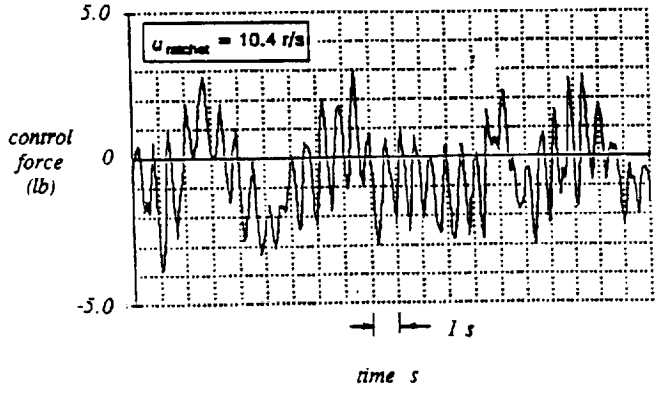

Fig. 9 Pilot inceptor force inputs from flight test of Ref. 4, as reported in Ref. 6, for configuration *143P(18)*.

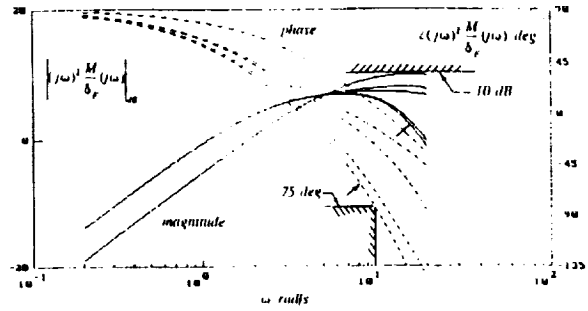

Fig. 10 $\left[s^2 \cdot \frac{M}{\delta_F}(s)\right]_{s=j\omega}$ for configurations in Ref. 6 identified as not experiencing roll ratchet.

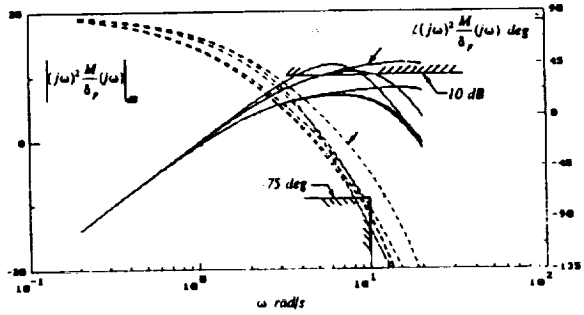

Fig. 11 $\left[s^2 \cdot \frac{M}{\delta_F}(s)\right]_{s=j\omega}$ for configurations in Ref. 6 identified as experiencing roll ratchet.

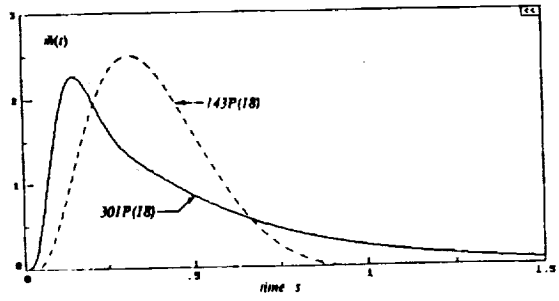

Fig. 12 Roll acceleration responses to step force inputs for configurations *301P(18)* (no ratchet) and *143P(18)* (ratchet).

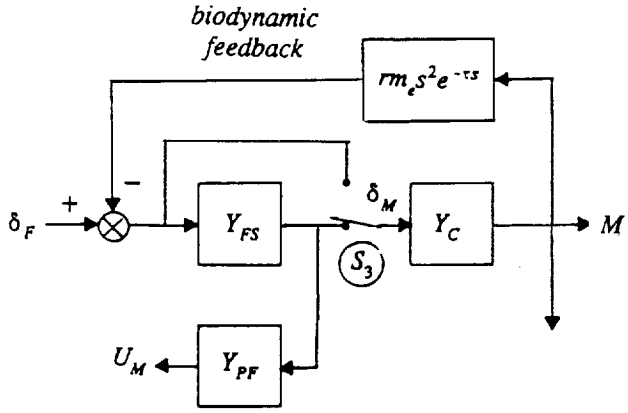

Fig. 13 Modification of Fig. 3 to model biodynamic feedback.

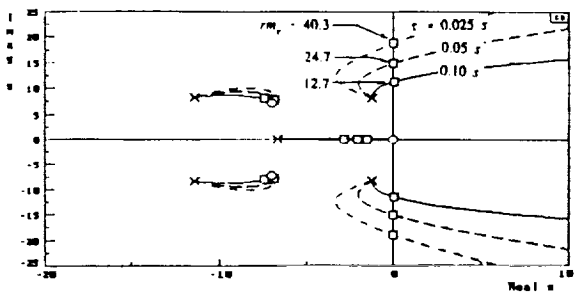

Fig. 14 Root locus diagrams for closed-loop poles of $\frac{M}{E_M}(s)$ for different τ values in biodynamic feedback model.